Supplementary Data and Methods

Non-opioid analgesia based on Gα signalling bias

Mark J. Wall, Emily Hill, Robert Huckstepp, Giuseppe Deganutti, Michele Leuenberger, Barbara Preti, Kerry Barkan, Ian Winfield, Haifeng Wei, Wendy Imlach, Eve Dean, Cherise Hume, Stephanie Hayward, Jess Oliver, Fei-Yue Zhao, David Spanswick, Christopher A. Reynolds, Martin Lochner, Graham Ladds and Bruno G. Frenguelli

Correspondence and requests for materials should be addressed to

Mark.Wall@warwick.ac.uk

Materials and Methods

Approvals. All experiments involving animals were conducted with the knowledge and approval of the University of Warwick Animal Welfare and Ethical Review Board, and in accordance with the U.K. Animals (Scientific Procedures) Act (1986) and the EU Directive 2010/63/EU. *In vivo* cardiorespiratory studies were conducted under the auspices of UK PPL 70/8936 and the chronic neuropathic pain studies under the auspices of P9D9428A9.

Preparation of hippocampal slices. Sagittal slices of hippocampus (300-400 μm) were prepared from male Sprague Dawley rats, at postnatal days 12-20 (*1*). Rats were kept on a 12-hour light-dark cycle with slices made 90 minutes after entering the light cycle. In accordance with the U.K. Animals (Scientific Procedures) Act (1986), rats were killed by cervical dislocation and then decapitated. The brain was removed, cut down the midline and the two sides of the brain stuck down to a metal base plate using cyanoacrylate glue. Slices were cut along the midline with a Microm HM 650V microslicer in cold (2-4°C) high Mg^{2+}, low Ca^{2+} aCSF, composed of (mM): 127 NaCl, 1.9 KCl, 8 $MgCl_2$, 0.5 $CaCl_2$, 1.2 KH_2PO_4, 26 $NaHCO_3$, 10 D-glucose (pH 7.4 when bubbled with 95% O_2 and 5% CO_2, 300 mOSM). Slices were stored at 34°C for 1-6 hours in aCSF (1 mM $MgCl_2$, 2 mM $CaCl_2$) before use.

Extracellular recording. A slice was transferred to the recording chamber, submerged in aCSF and perfused at 4-6 ml·min^{-1} (32 ± 0.5°C). The slice was placed on a grid allowing perfusion above and below the tissue and all tubing was gas tight (to prevent loss of oxygen). An aCSF-filled glass microelectrode was placed within stratum radiatum in area CA1 and recordings were made using either a differential model 3000 amplifier (AM

systems, WA USA) or a DP-301 differential amplifier (Warner Instruments, Hampden, CT USA). Field excitatory postsynaptic potentials (fEPSPs) were evoked with either an isolated pulse stimulator model 2100 (AM Systems, WA) or ISO-Flex (AMPI, Jerusalem, Israel). For fEPSPs a 10-20 minute baseline was recorded at a stimulus intensity that gave 40-50% of the maximal response. Signals were acquired at 10 kHz, filtered at 3 kHz and digitised on line (10 kHz) with a Micro CED (Mark 2) interface controlled by Spike software (Vs 6.1, Cambridge Electronic Design, Cambridge UK) or with WinLTP (*2*). For fEPSP slope, a 1 ms linear region after the fibre volley was measured. Extracellular recordings were made independently on two electrophysiology rigs. As the data obtained from each rig was comparable both sets of data have been pooled.

Seizure model. Seizure activity was induced in hippocampal slices using nominally Mg^{2+}-free aCSF that contained no added Mg^{2+} and with the total K^+ concentration increased to 6 mM with KCl. Removal of extracellular Mg^{2+} facilitates depolarisation via glutamate N-methyl-D-aspartate (NMDA) receptor activation. Increasing the extracellular concentration of K^+ depolarises neurons leading to firing and release of glutamate to sustain activity. Both the increase in K^+ concentration and removal of Mg^{2+} are required to produce spontaneous activity in hippocampal slices (*3*). Spontaneous activity was measured with an aCSF-filled microelectrode placed within stratum radiatum in area CA1.

Whole-cell patch clamp recording from hippocampal pyramidal cells. A slice was transferred to the recording chamber and perfused at 3 $ml \cdot min^{-1}$ with aCSF at 32 ± 0.5°C. Slices were visualized using IR-DIC optics with an Olympus BX151W microscope (Scientifica) and a CCD camera (Hitachi). Whole-cell current- and voltage-clamp recordings were made from pyramidal cells in area CA1 of the hippocampus using patch

pipettes (5–10 MΩ) manufactured from thick walled glass (Harvard Apparatus, Edenbridge UK) and containing (mM): potassium gluconate 135, NaCl 7, HEPES 10, EGTA 0.5, phosphocreatine 10, MgATP 2, NaGTP 0.3 and biocytin 1 mg ml^{-1} (290 mOSM, pH 7.2). Voltage and current recordings were obtained using an Axon Multiclamp 700B amplifier (Molecular Devices, USA) and digitised at 20 KHz. Data acquisition and analysis was performed using Pclamp 10 (Molecular Devices, USA). For voltage clamp experiments, CA1 pyramidal cells were held at -60 mV. Peptides to interfere with G protein signalling were introduced via the patch pipette into the recorded cell. The cell was held for at least 10 minutes before adenosine (10 μM) was added to induce an outward current.

Frog heart preparation. Young adult male *Xenopus leavis* frogs were obtained from Portsmouth Xenopus Resource Centre. Frogs were euthanized with MS222 (0.2 % at a pH of 7), decapitated and pithed. The animals were dissected to reveal the heart and the pericardium was carefully removed. Heart contractions were measured with a force transducer (AD instruments). Heart rate was acquired via a PowerLab 26T (AD instruments) controlled by LabChart 7 (AD instruments). The heart was regularly washed with Ringer solution and drugs were applied directly to the heart.

***In vivo* anaesthetised rat preparation for cardiorespiratory recordings:** Anaesthesia was induced in adult male Sprague Dawley rats (230-330 g) with isofluorane (2-4%; Piramal Healthcare). The femoral vein was catheterised for drug delivery. The trachea was cannulated and the femoral artery catheterised, and both were connected to pressure transducers (Digitimer) to record respiratory airflow and arterial blood pressure, respectively. Anaesthesia was maintained with urethane (1.2-1.7 $g \cdot kg^{-1}$; Sigma) in sterile

saline delivered via the femoral vein catheter. Body temperature was maintained at 36.7°C via a thermocoupled heating pad (TCAT 2-LV; Physitemp). The rats were allowed to stabilise before experiments began. Blood pressure and airflow signals were amplified using the NeuroLog system (Digitimer) connected to a micro1401 interface and acquired on a computer using Spike2 software (Cambridge Electronic Design). Arterial blood pressure recordings were used to derive heart rate (HR: beats.minute^{-1}; BPM), and to calculate mean arterial blood pressure (MAP: Diastolic pressure + ⅓*[Systolic Pressure - Diastolic pressure]). Airflow measurements were used to calculate: tidal volume (V_T; mL; pressure sensors were calibrated with a 3 mL syringe), and respiratory frequency (*f*; breaths·min^{-1}; BrPM). Minute ventilation (V_E; mL·min^{-1}) was calculated as *f* x V_T.

After allowing the animal to stabilise following surgery, A_1R agonists were administered by intravenous (IV) injection and the changes in HR, MAP, *f*, V_T, and V_E were measured. In pilot studies, the optimal dose of adenosine was determined by increasing the dose until robust and reliable changes in HR and MAP were produced (1 mg·kg^{-1}). The dose of CPA was adjusted until equivalent effects to adenosine were produced on HR and MAP (6.3 µg·kg^{-1}). For BnOCPA we initially used 5 µg·kg^{-1}, but saw no agonist effect on HR and MAP. To ensure this was not a false negative we increased the dose of BnOCPA (8.3 µg·kg^{-1}), which still gave no agonist effect on HR and MAP. However, as BnOCPA produced an antagonistic effect when co-administered with adenosine (Fig. 4; fig. S9B), it must have reached A_1Rs at a high enough concentration to be physiologically active. These observations confirmed that the lack of agonistic effects on HR and MAP were not due to a type II error. 8.3 µg·kg^{-1} BnOCPA was used for all further experiments. All injections were administered IV as a 350 µl·kg^{-1} bolus.

In the experimental study, rats received an injection of adenosine. After cardiorespiratory parameters returned to baseline (5-10 minutes) rats were given BnOCPA. After allowing sufficient time for any effect of BnOCPA to be observed, rats received adenosine with BnOCPA co-administered in a single injection. After cardiorespiratory parameters returned to baseline, rats were injected with CPA.

To check that the volume of solution injected with each drug did not itself induce a baroreflex response leading to spurious changes in cardiorespiratory responses, equivalent volumes of saline (0.9 %) were injected. These had no effect on either heart rate or MAP (fig. S9C). To confirm that repeated doses of adenosine produced the same response and that the responses did not run-down, rats were given two injections of adenosine (1 $mg \cdot kg^{-1}$). There was no significant difference in the changes in cardiovascular parameters produced by each adenosine injection (fig. S9D).

An additional series of experiments (n = 4) were undertaken to directly compare BnOCPA and CPA on respiration. Adult male Sprague Dawley rats (400-500 g) were anaesthetised with urethane and instrumented as described above, with the exception that the arterial cannulation was not performed.

After allowing the animal to stabilise following surgery, BnOCPA (8.3 $\mu g \cdot kg^{-1}$) was administered. After a 20 minutes recovery period CPA (6.3 $\mu g \cdot kg^{-1}$) was administered. All injections were administered IV as a 350 $\mu l \cdot kg^{-1}$ bolus. Changes in *f*, V_T, and V_E were measured. If the dosing occurred close to a respiratory event such as a sigh a second IV dose was administered, with 20 minute recovery periods either side of the injection. Measurements for the effect of BnOCPA were time-matched to when CPA induced a

change in respiration in the same preparation. As no difference was observed between the respiratory responses to BnOCPA in these rats (n = 4) and those instrumented for both cardiovascular and respiratory recordings (n = 4), the data were pooled (n = 8; Fig. 6A to D).

Spinal nerve ligation (Chung model (*4*)): Adult male Sprague-Dawley rats, 7-8 weeks old, weighing around 250 g at the time of Chung model surgery, were purchased from Charles River UK Ltd. The animals were housed in groups of 4 in an air-conditioned room on a 12-hour light/dark cycle. Food and water were available *ad libitum*. They were allowed to acclimatise to the experimental environment for three days by leaving them on a raised metal mesh for at least 40 min. The baseline paw withdrawal threshold (PWT) was examined using a series of graduated von Frey hairs (see below) for 3 consecutive days before surgery and re-assessed on the 6^{th} to 8^{th} day after surgery and on the 13^{th} to 17^{th} day after surgery before drug dosing.

Prior to surgery each rat was anaesthetized with 3% isoflurane mixed with oxygen (2 $L \cdot min^{-1}$) followed by an i.m. injection of ketamine (60 $mg \cdot kg^{-1}$) plus xylazine (10 $mg \cdot kg^{-1}$). The back was shaved and sterilized with povidone-iodine. The animal was placed in a prone position and a para-medial incision was made on the skin covering the L4-6 level. The L5 spinal nerve was carefully isolated and tightly ligated with 6/0 silk suture. The wound was then closed in layers after a complete hemostasis. A single dose of antibiotics (Amoxipen, 15 mg/rat, i.p.) was routinely given for prevention of infection after surgery. The animals were placed in a temperature-controlled recovery chamber until fully awake before being returned to their home cages. The vehicle (normal saline) was administered via the intravenous (IV) route at 1 $ml \cdot kg^{-1}$ and via the intrathecal (IT) route at 10 µl for

each injection. The rats with validated neuropathic pain state were randomly divided into 8 groups: vehicle IV, BnOCPA at 1, 3, 10 $\mu g \cdot kg^{-1}$ g IV; vehicle IT, BnOCPA at 0.3, 1, and 3 nmol IT groups.

To test for mechanical allodynia the animals were placed in individual Perspex boxes on a raised metal mesh for at least 40 minutes before the test. Starting from the filament of lower force, each filament was applied perpendicularly to the centre of the ventral surface of the paw until slightly bent for 6 seconds. If the animal withdrew or lifted the paw upon stimulation, then a hair with force immediately lower than that tested was used. If no response was observed, then a hair with force immediately higher was tested. The highest value was set at 15 g. The lowest amount of force required to induce reliable responses (positive in 3 out of 5 trials) was recorded as the value of PWT. On the testing day, PWT were assessed before and 1, 2 and 4 hours following BnOCPA or vehicle administration. The animals were returned to their home cages to rest (about 30 min) between two neighbouring testing time points. At the end of each experiment, the animals were deeply anaesthetised with isoflurane and killed by decapitation.

Rotarod test for motor function. A rotarod test was used to assess motor coordination following intravenous and intraperitoneal administration of BnOCPA. An accelerating rotarod (Ugo Basile) was set so speed increased from 6 to 80 rpm over 170 seconds. Male Sprague Dawley rats (n = 24), 7 weeks of age (212-258g) were trained on the rotarod twice daily for two days (≥2 trials per session) until performance times were stable. On the day of the experiment, three baseline trials were recorded. The compound was administered IP or intravenously via tail vein injection (10 μg/kg, n = 6 per group). The control group received subcutaneous saline and the positive control group received

subcutaneous morphine (15 mg/kg). Latency to fall (seconds) was measured in triplicate at 1, 2, 3 and 5 hours post drug administration.

Cell signaling assays. CHO-K1-hA_1R cells were routinely cultured in Hams F12 nutrient mix supplemented with 10% Foetal bovine serum (FBS), at 37°C with 5% CO_2, in a humidified atmosphere. For cAMP inhibition experiments, cells were seeded at a density of 2000 cells per well of a white 384-well optiplate and co-stimulated, for 30 minutes, with 1 µM forskolin and a range of agonist concentrations (1 µM – 1 pM). cAMP levels were then determined using a LANCE® cAMP kit as described previously (*5, 6*).

For determination of individual $G\alpha_{i/o/z}$ couplings, CHO-K1-hA_1R cells were transfected with pcDNA3.1-GNAZ or, pcDNA3.1 containing pertussis toxin (PTX) insensitive $G\alpha_{i/o}$ protein mutants (C351I, C352I, C351I, C351I, C351I, for G_{i1}, G_{i2}, G_{i3}, G_{oa}, G_{ob}, respectively, obtained from cDNA Resource Center; www.cdna.org), using 500 ng plasmid and Fugene HD at a 3:1 (Fugene:Plasmid) ratio. Cells were then incubated for 24 hours before addition of 100 ng/ml PTX, to inhibit activity of endogenous $G\alpha_{i/o}$, and then incubated for a further 16-18 hours. Transfected cells were then assayed as per cAMP inhibition experiments, but co-stimulated with agonist and 100 nM forskolin.

β-arrestin recruitment assays. HEK 293 cells were routinely grown in DMEM/F-12 GlutaMAX™ (Thermo Fisher Scientific) supplemented with 10% foetal bovine serum (FBS) (F9665, Sigma-Aldrich) and 1x antibiotic-antimycotic (Thermo Fisher Scientific) (DMEM complete). For analysis of β-arrestin2 recruitment following ligand stimulation at the human A_1R or A_3R, HEK 293 cells in a single well of 6-well plate (confluency ≥80%)

were transiently co-transfected with either A_1R-Nluc or A_3R-Nluc and β-arrestin2-YFP (total 2 µg, at a 1:6 ratio) using polyethyleneimine (PEI, 1 mg/ml, MW = 25,000 g/mol) (Polysciences Inc) at a DNA:PEI ratio of 1:6 (w/v). Briefly, in sterile tubes containing 150 mM sodium chloride (NaCl), DNA or PEI was added (final volume 50 µl), allowed to incubate at room temperature for 5 minutes, mixing together and incubating for a further 10 minutes prior to adding the combined mix dropwise to the cells. 24 hours post-transfection, HEK 293 cell were harvested, resuspended in reduced serum media (MEM, NEAA (Thermo Fisher Scientific) supplemented with 1% L-glutamine (2 mM final) (Thermo Fisher Scientific), 2% FBS and 1x antibiotic-antimycotic) and seeded (50,000 cells/well) in a poly-L-lysine-coated (MW 150,000-300,000, Sigma-Aldrich) white 96-well plate (PerkinElmer Life Sciences). 24 hours post seeding, media was removed, cells gently washed in PBS and 90 µl of furimazine (4 µM) containing solution added (PBS supplemented with 0.49 mM $MgCl_2$, 0.9 mM $CaCl_2$ and 0.1% BSA) to each well before incubating in the dark for 10 minutes. After incubation, 10 µl of ligand (NECA/CPA, adenosine, BnOCPA) was added in the range of 10 µM to 0.01 µM and filtered light emission measured at 450 nm and 530 nm every minute for 1 hour using a Mithras LB 940 (Berthold technology). Here, Nluc on the C-terminus of A_1R or A_3R acted as the BRET donor (luciferase oxidizing its substrate) and YFP acted as the fluorescent acceptor. Vehicle control (DMSO) was added to determine background emission.

Radioligand binding. Radioligand displacement assays were conducted using crude membrane preparations (100 µg protein per tube) acquired from homogenisation of CHO-K1-hA_1R cells in ice-cold buffer (2 mM $MgCl_2$, 20 mM HEPES, pH 7.4). The ability to displace binding of the A_1R selective antagonist radioligand, 1,3-[^{3}H]-dipropyl-8-

cyclopentylxanthine ([^{3}H]-DPCPX) at a concentration (1 nM) around the Kd value (1.23 nM, as determined by saturation binding experiments) by increasing concentrations of NECA, adenosine, CPA, BnOCPA or HOCPA (10 μM – 0.1 nM) allowed the binding affinities (Ki) to be determined. Non-specific binding was determined in the presence of 10 μM DPCPX. Membrane incubations were conducted in Sterilin™ scintillation vials (Thermo Fisher Scientific; Wilmington, Massachusetts, USA) for 60 minutes at room temperature. Free radioligand was separated from bound radioligand by filtration through Whatman® glass microfiber GF/B 25 mm filters (Sigma-Aldrich). Each filter was then placed in a Sterilin™ scintillation vial and radioactivity determined by: addition of 4 mL of Ultima Gold XR liquid scintillant (PerkinElmer), overnight incubation at room temperature and the retained radioactivity determined using a Beckman Coulter LS 6500 Multi-purpose scintillation counter (Beckman Coulter Inc.; Indiana, USA).

Data Analysis. Concentration-response curves for the effects of A_1R agonists on synaptic transmission were constructed in OriginPro 2018 (OriginLab; Northampton, MA, USA) and fitted with a logistic curve using the Levenberg Marquadt iteration algorithm. OriginPro 2018 was also used for statistical analysis. Statistical significance was tested as indicated in the text using paired or unpaired t-tests or one-way or two-way ANOVAs with repeated measures (RM) as appropriate. Bonferroni corrections for multiple comparisons were performed. All *in vitro* cell signalling assay data was analysed using Prism 7.0e (Graphpad software, San Diego, CA), with all concentration-response curves being fitted using a 3 parameter logistic equation to calculate response range and IC_{50}. All cAMP data was normalised to a forskolin concentration-response curve ran in parallel to each assay. Statistical significance to adenosine was calculated using a one-way

ANOVA with a Dunnett's post-test for multiple comparisons. Radioligand displacement curves were fitted to the one-site competition binding equation yielding logKi values. One-way ANOVA (Dunnett's post-test) was used to determine significance by comparing the logKi value for each compound when compared to adenosine. To determine the extent of ligand-induced recruitment of β-arrestin2-YFP to either the A_1R or A_3R, the BRET signal was calculated by subtracting the 530 nm/450 nm emission for vehicle-treated cells from ligand-treated cells (ligand-induced ΔBRET). ΔBRET for each concentration at 5 minutes (maximum response) was used to produce concentration-response curves.

All *in vivo* cardiovascular and respiratory data were analysed using OriginPro 2018. One-way ANOVAs, with repeated measures as appropriate, and with Bonferroni correction for multiple comparisons were used. Statistical significance for the effects of IV saline was tested using paired t-tests. Data are reported throughout as mean ± SEM and n values are reported for each experiment. For the neuropathic pain studies, one-way ANOVAs with Fisher's Least Significant Difference (LSD) post-hoc test was used to compare drug treatment groups to the vehicle group (OriginPro 2018). The significance level was set at $P < 0.05$, with actual P values reported in the figure legends and summaries, by way of abbreviations and asterisks, on the graphs: ns, not significant; ∗ $P < 0.05$; ∗∗, $P < 0.02$; ∗∗∗, $P < 0.001$; ∗∗∗∗, $P < 0.0001$.

Drugs and substances. Drugs were made up as stock solutions (1-10 mM) and then diluted in aCSF or saline on the day of use. BnOCPA (*7*) ((2*R*,3*R*,4*S*,5*R*)-2-(6-(((1*R*,2*R*)-2-(benzyloxy)cyclopentyl)amino)-9*H*-purin-9-yl)-5-(hydroxymethyl)tetrahydrofuran-3,4-diol) and HOCPA (*8*) ((2*R*,3*R*,4*S*,5*R*)-2-(6-(((1*R*,2*R*)-2-hydroxycyclopentyl)amino)-9*H*-purin-9-yl)-5-(hydroxymethyl)tetrahydrofuran-3,4-diol) were synthesised as described

previously (*5*) and dissolved in dimethyl-sulphoxide (DMSO, 0.01% final concentration). Adenosine, 8-CPT (8-cyclopentyltheophylline), NECA (5′-(*N*-Ethylcarboxamido) adenosine) and CPA (N^6-Cyclopentyladenosine) were purchased from Sigma-Aldrich (Poole, Dorset, UK). 1,3-[^{3}H]-dipropyl-8-cyclopentylxanthine ([^{3}H]-DPCPX) was purchased from PerkinElmer (Life and Analytical Sciences, Waltham, MA). Peptides for interfering with G protein signalling were obtained from Hello Bio (Bristol, UK) and were based on published sequences (*9*). For G_{oa} the peptide had a sequence of MGIANNLRGCGLY. The scrambled version was LNRGNAYLCIGMG. For G_{ob} the peptide had a sequence of MGIQNNLKYIGIC. Peptides were made up as stock solutions (2 mM) and stored at -20°C. The stock solutions were dissolved in filtered intracellular solution just before use.

Molecular Dynamics Simulations

Ligand parameterization. The CHARMM36 (*10, 11*)/CGenFF (*12-14*) force field combination was employed in all the molecular dynamic (MD) simulations performed. Initial topology and parameter files of BnOCPA, HOCPA, and PSB36 were obtained from the Paramchem webserver (*12*). Higher penalties were associated with a few BnOCPA dihedral terms, which were therefore optimized at the HF/6-31G* level of theory using both the high throughput molecular dynamics (HTMD) (*15*) parameterize functionality and the Visual Molecular Dynamics (VMD) (*16*) Force Field Toolkit (ffTK) (*17*), after fragmentation of the molecule. Short MD simulations of BnOCPA in water were performed to visually inspect the behavior of the optimized rotatable bonds.

Systems preparation for fully dynamic docking of BnOCPA and HOCPA. Coordinates of the A_1R in the active, adenosine- and G protein-bound state were retrieved

from the Protein Data Bank (*18, 19*) database (PDB ID 6D9H (*20*)). Intracellular loop 3 (ICL3) which is missing from PDB ID 6D9H was rebuilt using Modeller 9.19 (*21, 22*). The G protein, with the exception of the C-terminal helix (helix 5) of the G protein alpha subunit (the key region responsible for the receptor TM6 active-like conformation) was removed from the system as in previous work (*23, 24*). BnOCPA and HOCPA were placed in the extracellular bulk, in two different systems, at least 20 Å from the receptor vestibule. The resulting systems were prepared for simulations using in-house scripts able to exploit both python HTMD (*15*) and Tool Command Language (TCL) scripts. Briefly, this multistep procedure performs the preliminary hydrogen atoms addition by means of the pdb2pqr (*25*) and propka (*26*) software, considering a simulated pH of 7.0 (the proposed protonation of titratable side chains was checked by visual inspection). Receptors were then embedded in a square 80 Å x 80 Å 1-palmitoyl-2-oleyl-sn-glycerol-3-phosphocholine (POPC) bilayer (previously built by using the VMD Membrane Builder plugin 1.1, Membrane Plugin, Version 1.1.; http://www.ks.uiuc.edu/Research/vmd/plugins/membrane/) through an insertion method (*27*), considering the A_1R coordinates retrieved from the OPM database (*28*) to gain the correct orientation within the membrane. Lipids overlapping the receptor transmembrane bundle were removed and TIP3P water molecules (*29*) were added to the simulation box (final dimensions 80 Å × 80 Å × 125 Å) using the VMD Solvate plugin 1.5 (Solvate Plugin, Version 1.5; http://www.ks.uiuc.edu/Research/vmd/plugins/solvate/). Finally, overall charge neutrality was achieved by adding Na^+/Cl^- counter ions (concentration of 0.150 M) using the VMD Autoionize plugin 1.3 (Autoionize Plugin, Version 1.3; http://www.ks.uiuc.edu/Research/vmd/plugins/autoionize/). All histidine side chains were

considered in the delta tautomeric state, with the exception of H251 (epsilon tautomer) and H278 (protonated).

The MD engine ACEMD (*30*) was employed for both the equilibration and productive simulations. Systems were equilibrated in isothermal-isobaric conditions (NPT) using the Berendsen barostat (*31*) (target pressure 1 atm), the Langevin thermostat (*32*) (target temperature 300 K) with a low damping factor of 1 ps^{-1} and with an integration time step of 2 fs. Clashes between protein and lipid atoms were reduced through 2000 conjugate-gradient minimization steps before a 2 ns long MD simulation was run with a positional constraint of 1 kcal mol^{-1} $Å^{-2}$ on protein and lipid phosphorus atoms. Twenty nanoseconds of MD simulation were then performed constraining only the protein atoms. Lastly, positional constraints were applied only to the protein backbone alpha carbons for a further 5 ns.

Dynamic docking of BnOCPA and HOCPA. The supervised MD (SuMD) approach is an adaptive sampling method (*33*) for simulating binding events in a timescale one or two orders of magnitudes faster than the corresponding classical (unsupervised) MD simulations (*34*). SuMD has been successfully applied to small molecules and peptides (*35-41*). In the present work, the distances between the centers of mass of the adenine scaffold of the A_1R agonist and $N254^{6.55}$, $F171^{ECL2}$, $T277^{7.42}$ and $H278^{7.43}$ of the receptor were considered for the supervision during the MD simulations. The dynamic docking of BnOCPA was hindered by the ionic bridge formed between the $E172^{ECL2}$ and $K265^{ECL3}$ side chains. A metadynamics (*42-44*) energetic bias was therefore introduced in order to facilitate the rupture of this ionic interaction, thus favoring the formation of a bound complex. More precisely, Gaussian terms (height = 0.01 kcal mol^{-1} and widths = 0.1 Å)

were deposited every 1 ps along the distance between the $E172^{ECL2}$ carboxyl carbon and the positively charged $K265^{ECL3}$ nitrogen atom using PLUMED 2.3 (*45*). A similar SuMD-metadynamics hybrid approach was previously employed to study binding/unbinding kinetics (*46*) on the $A_{2A}R$ subtype. For each replica (Methods Table 1), when the ligands reached a bound pose (i.e. a distance between the adenine and the receptor residues centers of mass < 3 Å), a classic (unsupervised and without energetic bias) MD simulation was performed for at least a further 100 ns.

BnOCPA bound state metadynamics. We decided to perform a detailed analysis of the role played by the $E172^{ECL2}$ - $K265^{ECL3}$ ionic interaction in the dynamic docking of BnOCPA. Three 250 ns long well-tempered (*47*) metadynamics simulations were performed using the bound state obtained from a previous dynamic docking simulation, which resulted in binding mode A, as a starting point. The collective variables (CVs) considered were: i) the distance between the $E172^{ECL2}$ carboxyl carbon and the positively charged $K265^{ECL3}$ nitrogen atom and ii) the dihedral angle formed by the 4 atoms linking the cyclopentyl ring to the phenyl moiety (which was the most flexible ligand torsion during the previous SuMD simulations). Gaussian widths were set at 0.1 Å and 0.01 radians respectively, heights at 0.01 kcal/mol^{-1}, and the deposition was performed every 1 ps (bias-factor = 5). Although complete convergence was probably not reached, three replicas (Methods Table 1) allowed sampling of three main energetic minima on the energy surface (fig. S7); these correspond to the representative binding poses shown in Fig. 3D to F.

Classic MD simulations of BnOCPA binding modes A, B, C and D. To test the hypothesis that BnOCPA and HOCPA may differently affect TM6 and/or TM7 mobility

when bound to A_1R (and to further sample the stability of each BnOCPA binding mode), putative binding conformations A, B and C (Fig. 3) were superposed to the experimental A_1R active state coordinates with the modelled ICL3. This should have removed any A_1R structural artefacts, possibly introduced by metadynamics. As reference and control, two further systems were considered: i) the pseudo-apo A_1R and ii) the selective A_1R antagonist PSB36 (*48*) superposed in the same receptor active conformation (Methods Table 1). The BnOCPA binding mode D was modelled from mode B by rotating the dihedral angle connecting the cyclopentyl ring and the N6 nitrogen atom in order to point the benzyl of the agonist toward the hydrophobic pocket underneath ECL3 (Fig. 3G) delimited by $L253^{6.56}$, $T257^{6.52}$, $K265^{ECL3}$,$T270^{7.35}$, and $L269^{7.34}$. The G protein atoms were removed, and the resulting systems prepared for MD as reported above. A similar comparison was performed in a milestone study on the β_2 adrenergic receptor (*49*) which sought to describe the putative deactivation mechanism of the receptor.

Dynamic docking of the Goa, Gob and Gi2 GαCT helix. A randomly extracted frame from the classic MD performed on the BnOCPA:A1R complex was prepared for three sets of simulations placing the GαCT helix 5 (last 27 residues) of the Gα proteins Goa, Gob and Gi2 in the intracellular solvent bulk side of the simulation boxes. As a further control, a frame from the classic MD performed on the unbiased ligand HOCPA:A_1R complex was randomly extracted and prepared along with the Gob GαCT. The resulting four systems were embedded in a POPC membrane and prepared as reported above.

The different structural effects putatively triggered by BnOCPA and HOCPA on the recognition mechanism of Goa, Gob and Gi2 GαCT were studied by performing 10 SuMD replicas (Methods Table 1). During each replica (Video S3), the distance between the

centroid of the GαCT residues 348-352 and the centroid of the A1R residues D42$^{2.37}$, I232$^{6.33}$, and Q293$^{8.48}$ was supervised until it reached a value lower than 8 Å. A classic MD simulation was then run for a further 300 ns.

Classic MD simulations on the A_1R:Goa and Gob complexes. The A_1R cryo-EM structure (PDB ID 6D9H) was used as template for all the five systems simulated (Methods Table 1). The endogenous agonist adenosine was removed and HOCPA and BnOCPA (modes B and D) were inserted in the orthosteric site superimposing 6D9H to the systems prepared for the classic MD simulations in the absence of G protein. ICL3 was not modelled, nor were the missing part of the G protein α subunit. As subunits β and γ were removed, the Gα NT helix was truncated to residue 27 to avoid unnatural movements (NT is constrained by Gβ in 6D9H). The Gα subunit was mutated according to the Goa and Gob primary sequences (*50*) using in-house scripts. The resulting five systems (Methods Table 1) were embedded in a POPC membrane and prepared as reported above.

Analysis of the classic MD simulations. During the classic MD simulations that started from Modes A-C (Fig. 3D to F), BnOCPA had the tendency to explore the three conformations by rapidly interchanging between the three binding modes. In order to determine the effect exerted on the TM domain by each conformation, 21 μs of MD simulations (Methods Table 1 - BnOCPA mode A, BnOCPA mode B, BnOCPA mode C) were subjected to a geometric clustering. More precisely, a simulation frame was considered in pose A if the distance between the phenyl ring of BnOCPA and the I175^{ECL2} alpha carbon was less than 5 Å; in pose B if the distance between the phenyl ring of BnOCPA and the L258$^{6.59}$ alpha carbon was less than 6 Å, and in pose C if the distance

between the phenyl ring of BnOCPA and the Y271$^{7.36}$ alpha carbon was less than 6 Å. During the MD simulations started from mode D (Fig. 3G), a frame was still considered in mode D if the root mean square deviation (RMSD) of the benzyl ring to the starting equilibrated conformation was less than 3 Å. For each of the resulting four clusters, the RMSD of the GPCR conserved motif NPXXY (N$^{7.49}$ PIV Y$^{7.53}$ in the A_1R; fig. S8) was computed using Plumed 2.3 (*45*) considering the inactive receptor state as reference, plotting the obtained values as frequency distributions (Fig. 3I, J). Rearrangement of the NPXXY motif, which is located at the intracellular half of TM7, is considered one of the structural hallmarks of GPCR activation (*51*). Upon G protein binding, it moves towards the center of the receptor TM bundle (Fig. S8). Unlike other activation micro-switches (e.g. the break/formation of the salt bridge between R$^{3.50}$ and E$^{6.30}$), this conformational transition is believed to occur in timescales accessible to MD simulations (*49*).

Hydrogen bonds and atomic contacts were computed using the GetContacts analysis tool (https://github.com/getcontacts/getcontacts) and expressed in terms of occupancy (the percentage of MD frames in which the interaction occurred).

Analysis of the Goa, Gob and Gi2 GαCT classic MD simulations after SuMD. For each system, only the classic MD simulations performed after the GαCT reached the A1R intracellular binding site were considered for the analysis.

The RMSD values to the last 15 residues of the Gi2 GαCT reported in the A_1R cryo-EM PDB structure 6D9H were computed using VMD (*16*). The MD frames associated with the peaks in the RMSD plots (states CS1, MS1, MS2 and MS3 in Fig. 4A, D) were

clustered employing the VMD Clustering plugin (https://github.com/luisico/clustering) by selecting the whole GαCT helixes alpha carbon atoms and a cutoff of 3 Å.

Methods Table 1. Summary of the simulations performed.

Ligand	MD approach	# Replicas	Total simulated time[a]
BnOCPA	**SuMD**	**6**	**1.9 μs**
BnOCPA	**SuMD-Metadynamics**	**5**	**4.3 μs**
HOCPA	**SuMD**	**5**	**3.4 μs**
BnOCPA (bound state after dynamic docking)	**Metadynamics**	**3**	**0.75 μs**
BnOCPA(A)	**Classic MD**	**6**	**9.0 μs**
BnOCPA(B)	**Classic MD**	**6**	**9.0 μs**
BnOCPA(C)	**Classic MD**	**3**	**3.0 μs**
HOCPA	**Classic MD**	**4**	**8.0 μs**
PSB36	**Classic MD**	**4**	**6.0 μs**
Apo A_1	**Classic MD**	**4**	**8.0 μs**
GαCT Goa (BnOCPA)	**SuMD + Classic MD**	**10**	**0.36 μs + 3.0 μs**
GαCT Gob (BnOCPA)	**SuMD + Classic MD**	**10**	**0.33 μs + 3.0 μs**
GαCT Gi2 (BnOCPA)	**SuMD + Classic MD**	**10**	**0.37 μs + 3.0 μs**
GαCT Gob (HOCPA)	**SuMD + Classic MD**	**10**	**0.29 μs + 3.0 μs**
BnOCPA(D):Gob	**Classic MD**	**4**	**4.0 μs**
BnOCPA(B):Gob	**Classic MD**	**3**	**3.0 μs**
HOCPA:Gob	**Classic MD**	**4**	**4.0 μs**
BnOCPA(D):Goa	**Classic MD**	**5**	**5.0 μs**
BnOCPA(B):Goa	**Classic MD**	**4**	**4.0 μs**

a) For SuMD and SuMD-metadynamics simulations the time is the sum of productive SuMD time windows.

(A), (B), (C) and (D) indicate the respective BnOCPA binding modes.

Supplementary Methods References

1. M. J. Wall, N. Dale, Neuronal transporter and astrocytic ATP exocytosis underlie activity-dependent adenosine release in the hippocampus. *J.Physiol* **591**, 3853-3871 (2013).
2. W. W. Anderson, G. L. Collingridge, Capabilities of the WinLTP data acquisition program extending beyond basic LTP experimental functions. *J.Neurosci.Methods* **162**, 346-356 (2007).
3. B. G. Frenguelli, M. J. Wall, Combined electrophysiological and biosensor approaches to study purinergic regulation of epileptiform activity in cortical tissue. *J Neurosci Methods* **260**, 202-214 (2016).
4. S. H. Kim, J. M. Chung, An experimental model for peripheral neuropathy produced by segmental spinal nerve ligation in the rat. *Pain* **50**, 355-363 (1992).
5. A. Knight *et al.*, Discovery of novel adenosine receptor agonists that exhibit subtype selectivity. *J Med Chem* **59**, 947-964 (2016).
6. C. Weston *et al.*, Receptor activity-modifying protein-directed G protein signaling specificity for the calcitonin gene-related peptide family of receptors. *J Biol Chem* **291**, 25763 (2016).
7. P. Jagtap, in *WO2011/119919 A1,* W. I. P. Organization, Ed. (2011), vol. WO2011/119919 A1, chap. WO2011/119919 A1, pp. WO2011/119919 A119911.
8. B. Evans*,* E. P. Office, Ed. (1989).
9. A. Gilchrist, A. Li, H. E. Hamm, G alpha COOH-terminal minigene vectors dissect heterotrimeric G protein signaling. *Sci STKE* **2002**, pl1 (2002).

10. J. Huang, A. D. MacKerell, CHARMM36 all-atom additive protein force field: validation based on comparison to NMR data. *J Comput Chem* **34**, 2135-2145 (2013).
11. J. Huang *et al.*, CHARMM36m: an improved force field for folded and intrinsically disordered proteins. *Nat Methods* **14**, 71-73 (2017).
12. K. Vanommeslaeghe, A. D. MacKerell, Jr., Automation of the CHARMM General Force Field (CGenFF) I: bond perception and atom typing. *J Chem Inf Model* **52**, 3144-3154 (2012).
13. K. Vanommeslaeghe, E. P. Raman, A. D. MacKerell, Automation of the CHARMM General Force Field (CGenFF) II: assignment of bonded parameters and partial atomic charges. *J Chem Inf Model* **52**, 3155-3168 (2012).
14. W. Yu, X. He, K. Vanommeslaeghe, A. D. MacKerell, Extension of the CHARMM General Force Field to sulfonyl-containing compounds and its utility in biomolecular simulations. *J Comput Chem* **33**, 2451-2468 (2012).
15. S. Doerr, M. J. Harvey, F. Noé, G. De Fabritiis, HTMD: High-Throughput Molecular Dynamics for Molecular Discovery. *J Chem Theory Comput* **12**, 1845-1852 (2016).
16. W. Humphrey, A. Dalke, K. Schulten, VMD: visual molecular dynamics. *J Mol Graph* **14**, 33-38, 27-38 (1996).
17. C. G. Mayne, J. Saam, K. Schulten, E. Tajkhorshid, J. C. Gumbart, Rapid parameterization of small molecules using the Force Field Toolkit. *J Comput Chem* **34**, 2757-2770 (2013).

18. H. Berman, K. Henrick, H. Nakamura, Announcing the worldwide Protein Data Bank. *Nat Struct Biol* **10**, 980 (2003).

19. H. M. Berman *et al.*, The Protein Data Bank. *Nucleic Acids Res* **28**, 235-242 (2000).

20. C. J. Draper-Joyce *et al.*, Structure of the adenosine-bound human adenosine A1 receptor-Gi complex. *Nature* **558**, 559-563 (2018).

21. A. Fiser, A. Sali, Modeller: generation and refinement of homology-based protein structure models. *Meth Enzymol* **374**, 461-491 (2003).

22. A. Sali, T. L. Blundell, Comparative protein modelling by satisfaction of spatial restraints. *J Mol Biol* **234**, 779-815 (1993).

23. E. Dal Maso *et al.*, Extracellular loops 2 and 3 of the calcitonin receptor selectively modify agonist binding and efficacy. *Biochemical Pharmacology* **150**, 214-244 (2018).

24. Y.-L. Liang *et al.*, Cryo-EM structure of the active, Gs-protein complexed, human CGRP receptor. *Nature* **561**, 492-497 (2018).

25. T. J. Dolinsky, J. E. Nielsen, J. A. McCammon, N. A. Baker, PDB2PQR: an automated pipeline for the setup of Poisson-Boltzmann electrostatics calculations. *Nucleic Acids Res* **32**, W665-667 (2004).

26. M. H. M. Olsson, C. R. Søndergaard, M. Rostkowski, J. H. Jensen, PROPKA3: Consistent Treatment of Internal and Surface Residues in Empirical pK Predictions. *J Chem Theory Comput* **7**, 525-537 (2011).

27. B. Sommer, Membrane Packing Problems: A short Review on computational Membrane Modeling Methods and Tools. *Comput Struct Biotechnol J* **5**, e201302014 (2013).

28. M. A. Lomize, A. L. Lomize, I. D. Pogozheva, H. I. Mosberg, OPM: orientations of proteins in membranes database. *Bioinformatics* **22**, 623-625 (2006).

29. W. L. Jorgensen, J. Chandrasekhar, J. D. Madura, R. W. Impey, M. L. Klein, Comparison of simple potential functions for simulating liquid water. *J. Chem. Phys.* **79**, 926 (1983).

30. M. J. Harvey, G. Giupponi, G. D. Fabritiis, ACEMD: Accelerating Biomolecular Dynamics in the Microsecond Time Scale. *J Chem Theory Comput* **5**, 1632-1639 (2009).

31. H. J. C. Berendsen, J. P. M. Postma, W. F. van Gunsteren, A. DiNola, J. R. Haak, Molecular dynamics with coupling to an external bath. *J. Chem. Phys.* **81**, 3684 (1984).

32. R. J. Loncharich, B. R. Brooks, R. W. Pastor, Langevin dynamics of peptides: the frictional dependence of isomerization rates of N-acetylalanyl-N'-methylamide. *Biopolymers* **32**, 523-535 (1992).

33. G. Deganutti, S. Moro, Estimation of kinetic and thermodynamic ligand-binding parameters using computational strategies. *Future Med Chem* **9**, 507-523 (2017).

34. D. Sabbadin, V. Salmaso, M. Sturlese, S. Moro, *Supervised molecular dynamics (sumd) approaches in drug design*. (2018), vol. 1824, pp. 287-298.

35. A. Cuzzolin *et al.*, Deciphering the Complexity of Ligand-Protein Recognition Pathways Using Supervised Molecular Dynamics (SuMD) Simulations. *J Chem Inf Model* **56**, 687-705 (2016).

36. G. Deganutti, A. Cuzzolin, A. Ciancetta, S. Moro, Understanding allosteric interactions in G protein-coupled receptors using Supervised Molecular Dynamics: A prototype study analysing the human A3 adenosine receptor positive allosteric modulator LUF6000. *Bioorg Med Chem* **23**, 4065-4071 (2015).

37. G. Deganutti, S. Moro, Supporting the Identification of Novel Fragment-Based Positive Allosteric Modulators Using a Supervised Molecular Dynamics Approach: A Retrospective Analysis Considering the Human A2A Adenosine Receptor as a Key Example. *Molecules* **22**, (2017).

38. G. Deganutti, V. Salmaso, S. Moro, Could Adenosine Recognize its Receptors with a Stoichiometry Other than 1 : 1? *Mol Inform* **37**, (2018).

39. G. Deganutti, A. Welihinda, S. Moro, Comparison of the Human A2A Adenosine Receptor Recognition by Adenosine and Inosine: New Insight from Supervised Molecular Dynamics Simulations. *ChemMedChem* **12**, 1319-1326 (2017).

40. D. Sabbadin, S. Moro, Supervised molecular dynamics (SuMD) as a helpful tool to depict GPCR-ligand recognition pathway in a nanosecond time scale. *J Chem Inf Model* **54**, 372-376 (2014).

41. V. Salmaso, M. Sturlese, A. Cuzzolin, S. Moro, Exploring Protein-Peptide Recognition Pathways Using a Supervised Molecular Dynamics Approach. *Structure* **25**, 655-662.e652 (2017).

42. D. Branduardi, F. L. Gervasio, M. Parrinello, From A to B in free energy space. *J Chem Phys* **126**, 054103 (2007).

43. A. Laio, M. Parrinello, Escaping free-energy minima. *Proc Natl Acad Sci USA* **99**, 12562-12566 (2002).

44. A. Laio, A. Rodriguez-Fortea, F. L. Gervasio, M. Ceccarelli, M. Parrinello, Assessing the accuracy of metadynamics. *J Phys Chem B* **109**, 6714-6721 (2005).

45. G. A. Tribello, M. Bonomi, D. Branduardi, C. Camilloni, G. Bussi, PLUMED 2: New feathers for an old bird. *Comput Phys Commun* **185**, 604-613 (2014).

46. G. Deganutti *et al.*, Impact of protein–ligand solvation and desolvation on transition state thermodynamic properties of adenosine A2A ligand binding kinetics. *In Silico Pharmacol* **5**, 16 (2016).

47. A. Barducci, G. Bussi, M. Parrinello, Well-tempered metadynamics: a smoothly converging and tunable free-energy method. *Phys Rev Lett* **100**, 020603 (2008).

48. R. K. Y. Cheng *et al.*, Structures of Human A1 and A2A Adenosine Receptors with Xanthines Reveal Determinants of Selectivity. *Structure* **25**, 1275-1285.e1274 (2017).

49. R. O. Dror *et al.*, Activation mechanism of the β2-adrenergic receptor. *Proc Natl Acad Sci USA* **108**, 18684-18689 (2011).

50. M. Jiang, N. S. Bajpayee, Molecular mechanisms of Go signaling. *Neurosignals* **17**, 23-41 (2009).

51. D. M. Rosenbaum, S. G. Rasmussen, B. K. Kobilka, The structure and function of G-protein-coupled receptors. *Nature* **459**, 356-363 (2009).

Supplementary Figures 1 - 10

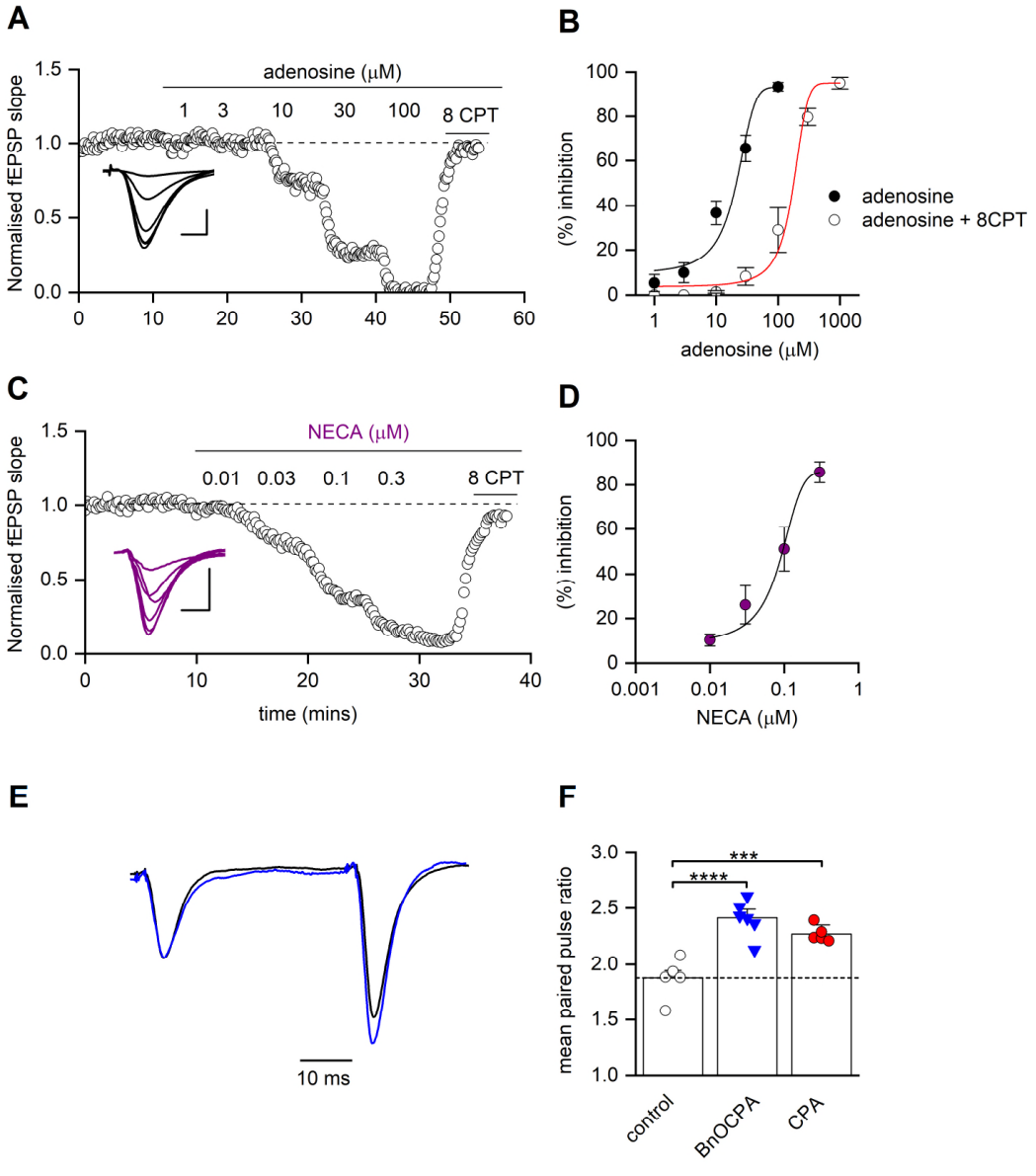

Fig. S1. A_1R agonists inhibit excitatory synaptic transmission at hippocampal synapses.

(A), Increasing concentrations of adenosine reduced fEPSP slope, an effect reversed by the A_1R antagonist 8CPT (2 μM). Inset, superimposed fEPSP averages in control and in increasing concentrations of adenosine. Scale bar measures 5 ms and 0.25 mV. **(B)**, Concentration-response curve for adenosine (IC_{50} = 20 ± 4.3 μM, *n* =11 slices) and for

adenosine with 2 μM 8CPT (IC_{50} = 125 ± 10 μM *n* = 5 slices). **(C)**, Increasing concentrations of the A_1R agonist NECA reduced fEPSP slope, an effect reversed by 8CPT (2 μM). Inset, superimposed fEPSP averages in control and in increasing concentrations of NECA. Scale bar measures 5 ms and 0.25 mV. **(D)**, Concentration-response curve for NECA (IC_{50} = 8.3 ± 3 nM, *n* =11 slices). **(E)**, Example of average (5 traces) superimposed paired-pulse fEPSP waveforms (50 ms inter-pulse interval) in control (black trace) and in the presence of BnOCPA (100 nM; blue trace). The fEPSP waveforms have been normalised to the amplitude of the first fEPSP in control. BnOCPA increased paired-pulse facilitation, indicative of a BnOCPA-induced reduction in the probability of glutamate release. **(F)**, Data summary. For a paired-pulse interval of 50 ms, the paired-pulse ratio was significantly increased (one-way ANOVA; F(2, 14) = 21.72; P = 5.11 x 10^{-5}) from 1.88 ± 0.07 in control (*n* = 6 slices) to 2.41 ± 0.07 in BnOCPA (*n* = 6 slices, P = 5.17 x 10^{-5}) and 2.27 ± 0.03 in CPA (60 nM; *n* = 5, P = 0.001). Averaged data is presented as mean ± SEM. ***, P < 0.001; ****, P < 0.0001.

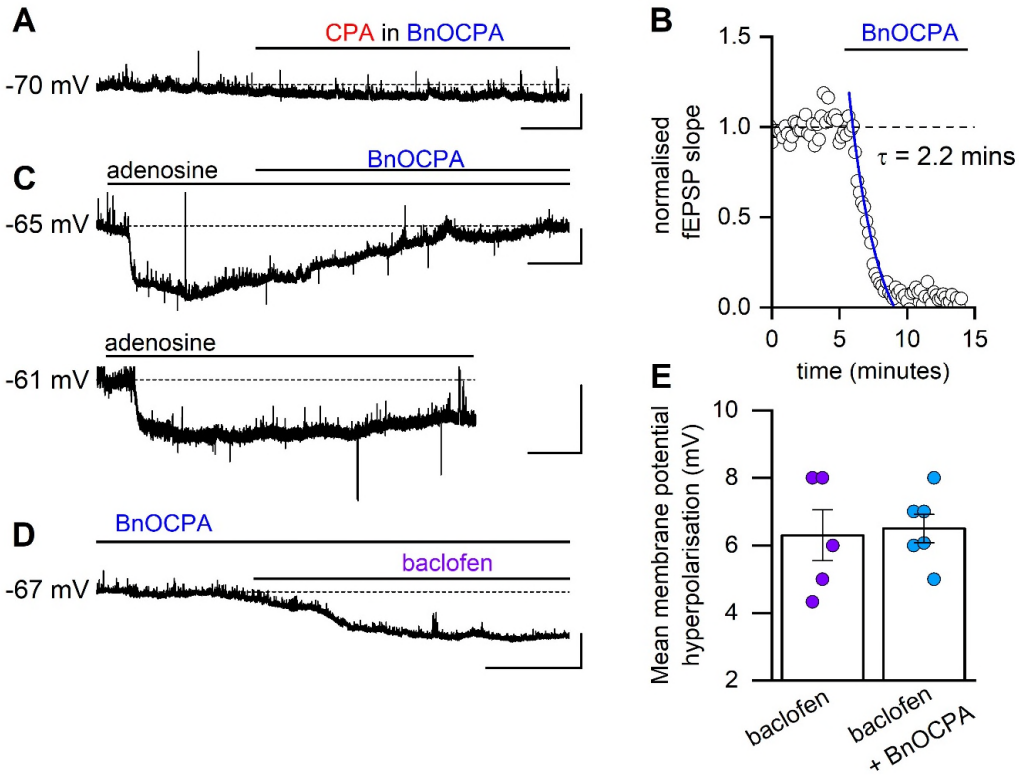

Fig. S2. Selective action of BnOCPA on membrane hyperpolarisation induced by prototypical A_1R agonists versus that induced by the $GABA_B$ receptor agonist baclofen.

(A), Membrane potential trace recorded from a CA1 pyramidal cell. BnOCPA (300 nM) reduced the effect of CPA (300 nM; quantified in main text Fig. 1H). **(B),** The same solution of BnOCPA (300 nM), which had no effect on membrane potential, abolished synaptic transmission in a sister slice (inhibition fitted with a single exponential; τ = 2.2 mins). **(C)**, BnOCPA reversed the hyperpolarising effect of adenosine (100 μM; similar observations were made in 3 other cells), which (lower trace) cannot be accounted for by fatigue of adenosine-mediated hyperpolarisation (similar observations of sustained hyperpolarisations to adenosine were made in 2 other cells). **(D)**, Application of baclofen (10 μM) in the presence of BnOCPA (300 nM) hyperpolarised the membrane potential (from -67 to -74 mV). Scale bars measure 5 mV and 50 s (CPA), 200 s (adenosine) or 100 s (baclofen). **(E)**, Data summary of baclofen/BnOCPA experiments. The mean hyperpolarisation produced by baclofen in the presence of BnOCPA was not significantly different (unpaired t-test) from that produced by baclofen in control conditions (6.5 ± 0.43 mV vs 6.3 ± 0.76 mV, P = 0.774, *n* = 5 - 6 cells for each condition). Bar chart displays individual data points and mean ± SEM.

Table S1 A_1R agonist binding and inhibition of cAMP production

	Binding	cAMP inhibition	
	pK_i[a]	pIC_{50}[b]	Range[c]
NECA	**6.45 ± 0.06*****	**9.65 ± 0.2*****	**61.21 ± 4.0**
Adenosine	**5.02 ± 0.10**	**8.46 ± 0.2**	**49.26 ± 4.1**
CPA	**6.65 ± 0.14*****	**9.26 ± 0.2*****	**48.97 ± 1.8**
BnOCPA	**6.58 ± 0.11*****	**9.17 ± 0.2*****	**55.28 ± 3.6**
HOCPA	**5.81 ± 0.16*****	**9.08 ± 0.1****	**60.52 ± 1.5**

Average data ± SEM of 4 - 19 individual replicates

[a] Negative logarithm of agonist concentration displacing 50% bound [^{3}H]-DPCPX.

[b] Negative logarithm of agonist concentration producing half-maximal response

[c] Range of response observed upon agonist stimulation, as a percentage of response obtained upon stimulation with 100 µM forskolin

Statistical difference between each agonist and adenosine was calculated using a one-way ANOVA with Dunnett's post-test (** $P < 0.01$; *** $P < 0.001$).

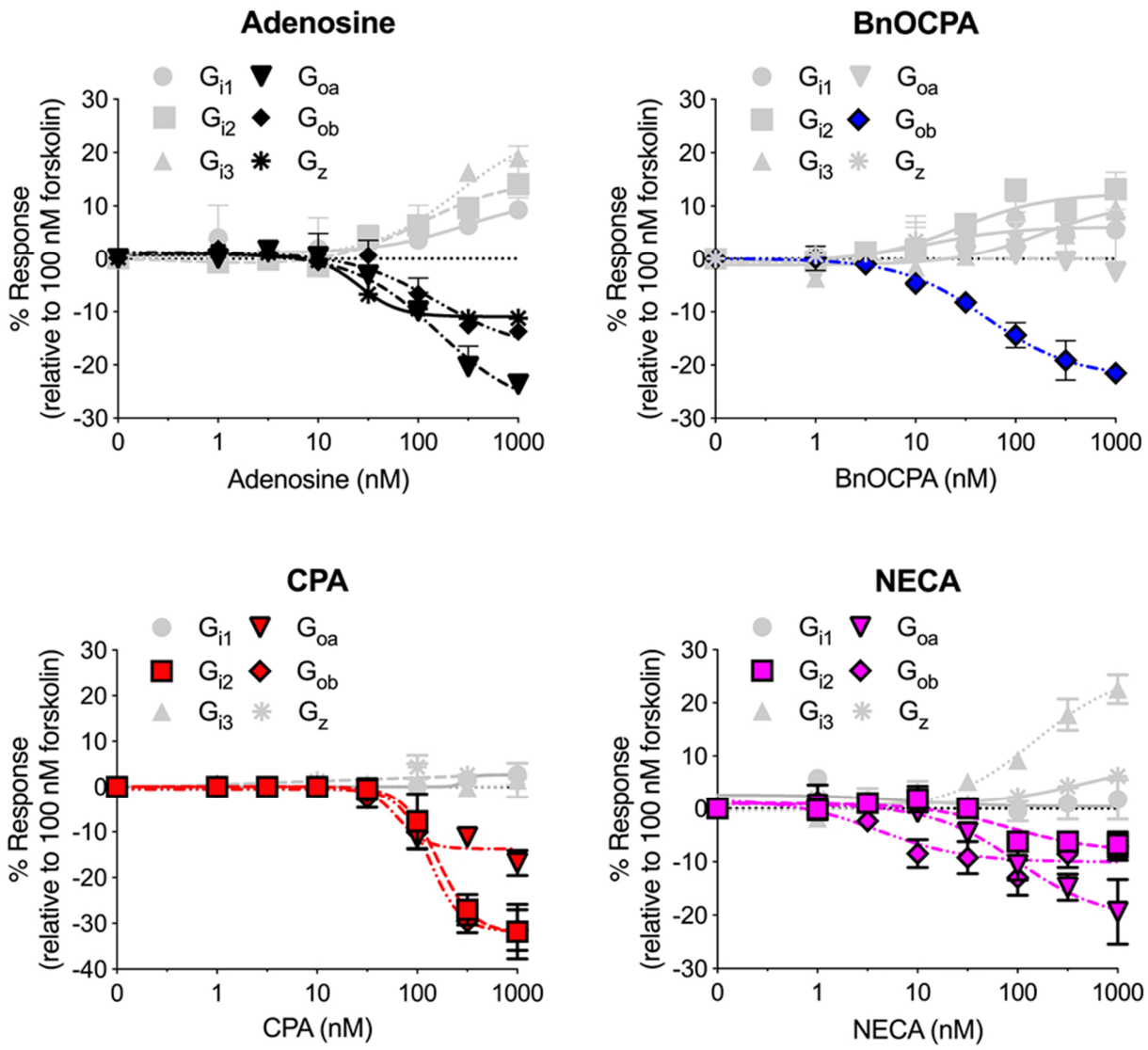

Fig. S3. Prototypical and atypical A_1R agonists display differing Gi/o activation profiles.

The ability of adenosine, BnOCPA, CPA and NECA to activate each individual Gi/o/z subtype was determined in CHO-K1-hA_1R cells, transfected with PTX-insensitive G proteins. cAMP levels were measured following 30 minute co-stimulation with 100 nM forskolin and each agonist. Adenosine displayed an ability to inhibit cAMP production via activation of Gi2, Goa, Gob, and Gz; CPA and NECA via Gi2, Goa and Gob, and BnOCPA exclusively via Gob. Data represented as the average level of cAMP production relative to that observed upon stimulation with 100 nM forskolin, ± SEM, of *n* = 4 - 6 individual replicates. Stimulation of cAMP production reflects activation of endogenous Gs by the A_1R and is in agreement with previous observations (*1-3*).

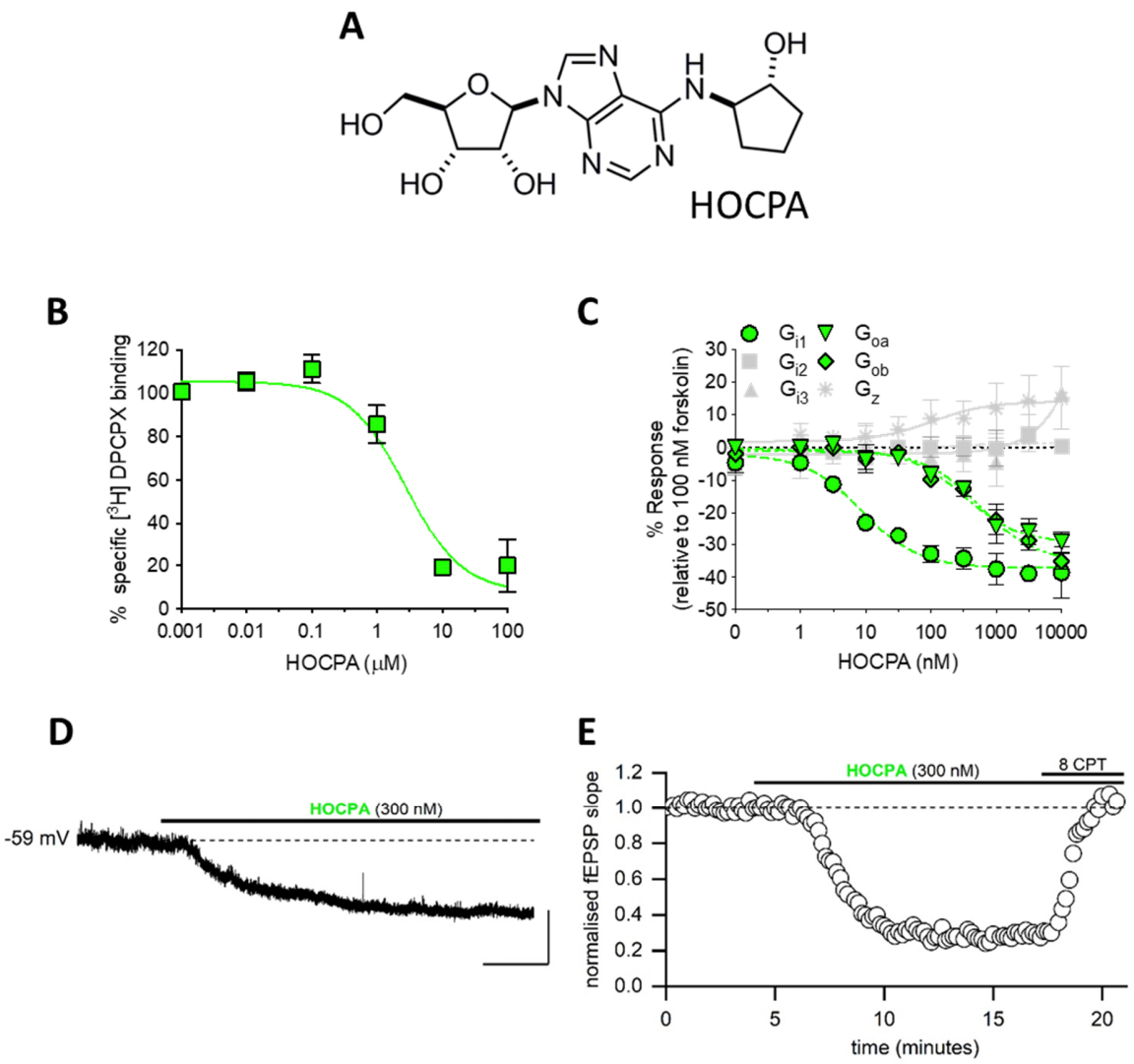

Fig. 4. HOCPA does not show signalling bias.

(A). Chemical structure of HOCPA. **(B)**, Binding of HOCPA was measured via its ability to displace [^{3}H]DPCPX from CHO-K1-hA_1R cells membranes. **(C)**, The ability of HOCPA to inhibit forskolin-stimulated (100 nM) cAMP production in PTX pre-treated (200 ng/ml) CHO-K1-hA_1R cells, transfected with PTX-insensitive Gi1, Gi2, Gi3, Goa, Gob or Gz. In contrast to BnOCPA, HOCPA shows no bias between Goa and Gob. All data are presented as mean ± SEM, of *n* = 4 - 5 individual replicates. **(D)**, Example membrane potential trace. HOCPA (300 nM) induced hyperpolarisation (mean hyperpolarisation 5.3 ± 0.5 mV, n = 6 cells). Scale bars measure 5 mV and 50 s. **(E)**, Graph plotting normalised fEPSP slope against time for a single experiment. HOCPA caused a ~80 % reduction in fEPSP slope, which was reversed by the A_1R antagonist 8CPT (4 μM). Similar results were observed in 4 slices.

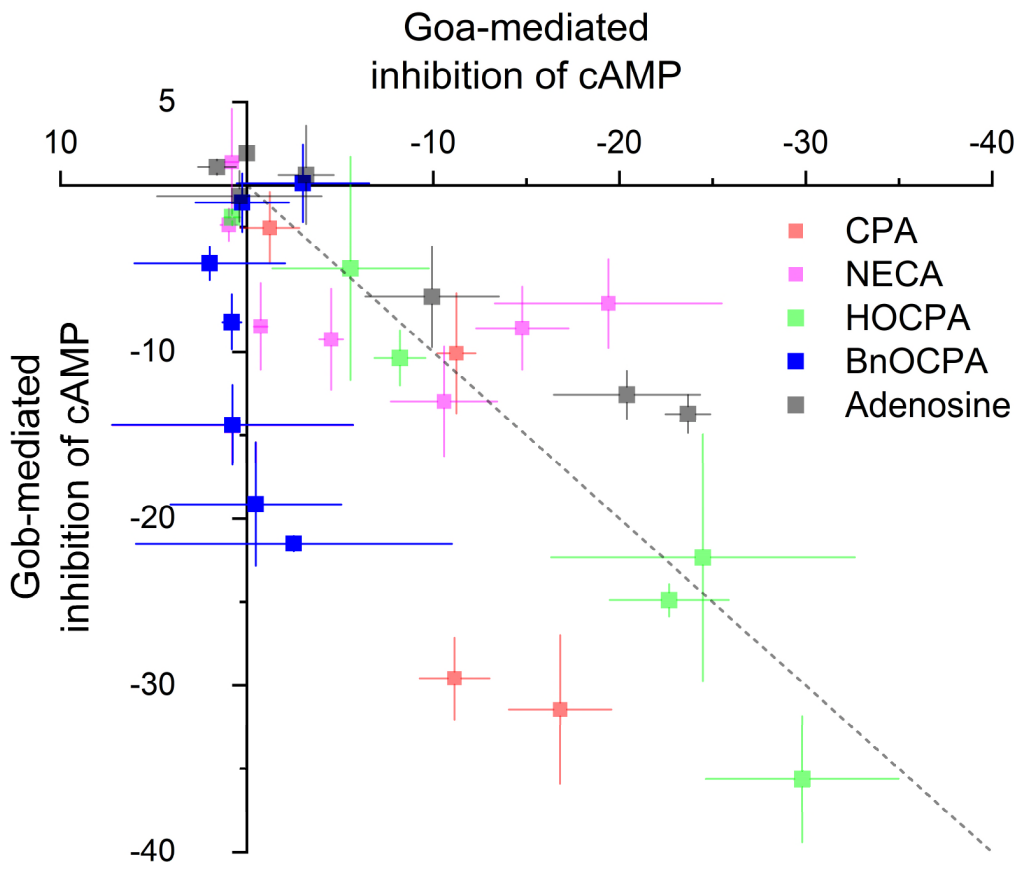

Fig. S5 Bias plot of Goa and Gob activation by the agonist-bound A_1R.
The inhibition of cAMP accumulation via A_1R:Goa or A_1R:Gob by A_1R agonists is plotted at each concentration of agonist. No bias (equal activation of Goa and Gob at each concentration) would fall on the line of identity (broken grey line). HOCPA behaves most like an unbiased agonist, with some bias for Gob shown by CPA, and for Goa by adenosine. NECA displays concentration-dependent bias at both Goa and Gob. BnOCPA is highly biased towards Gob. Data presented as mean ± SEM and is replotted from figs. S3 and S4.

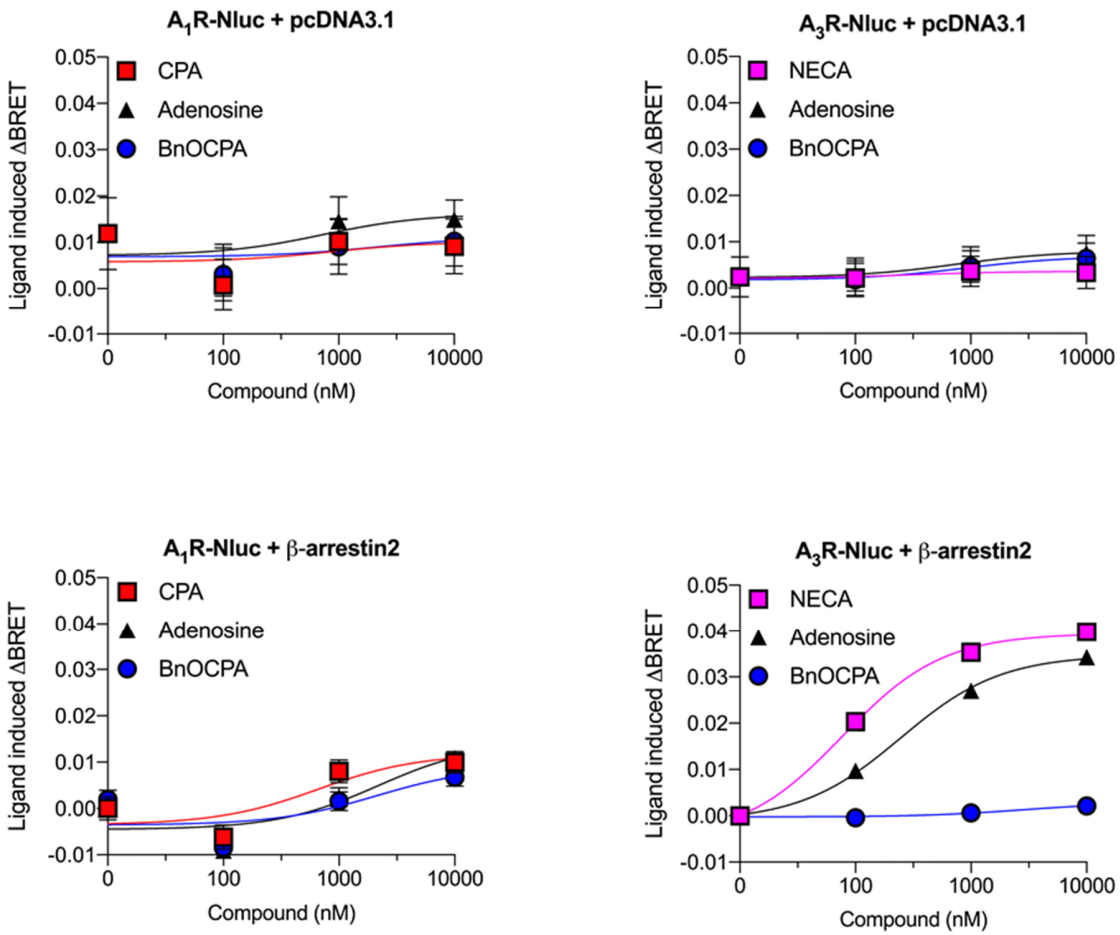

Fig. S6. β-arrestin2 recruitment to the A_1R or A_3R.

Interaction was detected using BRET between a C-terminally tagged Nluc GPCR (A_1R or A_3R) and β-arrestin2 C-terminal tagged with Venus-YFP. Note lack of β-arrestin2 recruitment to the A_1R either by adenosine, CPA or BnOCPA, which yields BRET signals comparable to the vector control experiments (pcDNA3.1). A_3R recruitment of β-arrestin2 is provided as a positive control for the BRET assay.

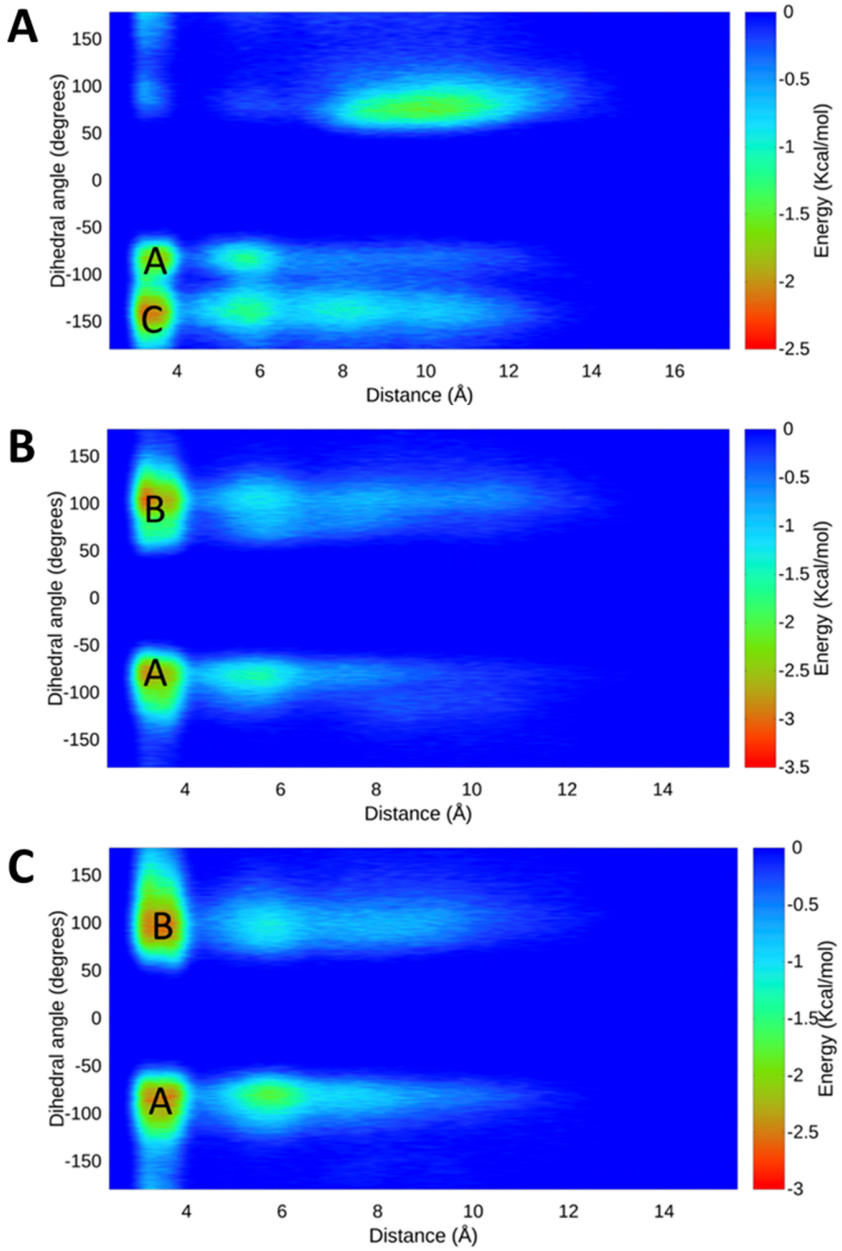

Fig. S7. Energy surfaces obtained from metadynamics simulations of BnOCPA. Energy surface obtained by integrating the Gaussian terms deposited during three well-tempered metadynamics replicas (panels **A**, **B** and **C**). X axes report the distance between the E172^{ECL2} carboxyl carbon and the positively charged K265^{ECL3} nitrogen atom; Y axes indicate the dihedral angle formed by the 4 atoms linking BnOCPA cyclopentyl ring to the phenyl moiety. The three energy minima (A, B and C) correspond to the three binding modes proposed for BnOCPA (Modes A, B, C in Fig. 3D to F, respectively).

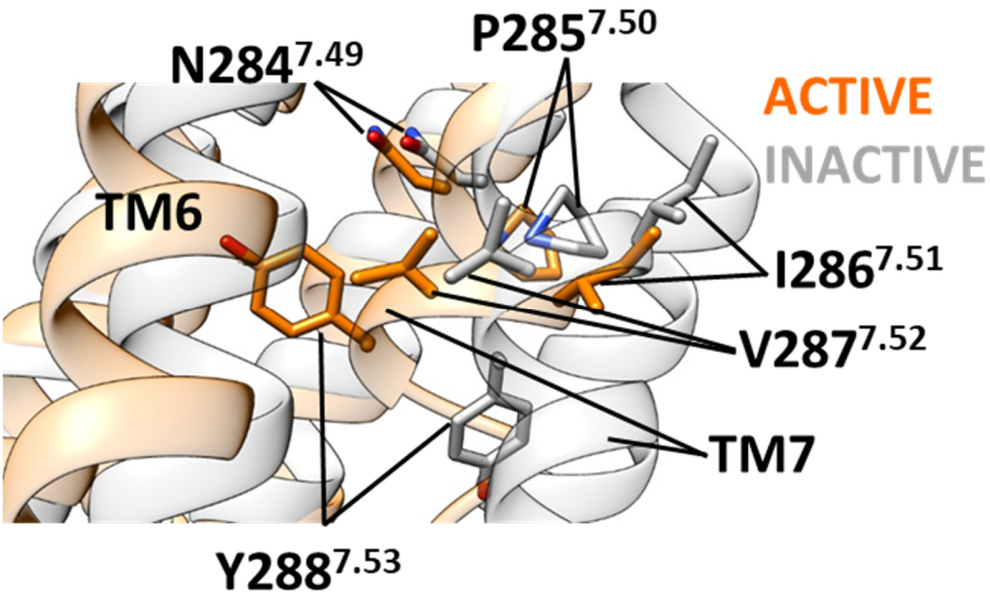

Fig. S8. The conserved NPXXY motif ($N^{7.49}$ PIV $Y^{7.53}$) in the A_1R.
The root mean square deviation (RMSD) was computed with respect to the A_1R inactive conformation. Compared to the inactive conformation (grey), in the active state (orange) the distal portion of TM7 is moved towards the TM bundle core (which is responsible for G protein binding). Starting from the active conformation (orange) and in absence of bound G protein, simulations should allow the structure to partially relax towards the inactive state (grey) with a dynamic influenced by the orthosteric ligand.

Table S2. Transient hydrogen bonds between α4-β6 loop residue 317 (N317 in Goa, H317 in Gob), the α3-β5 loop residue D263, and the residue on H8 of the A_1R (Ballesteros Weinstein enumeration in superscript).

A_1R - Gα Interactions					
	Coupling Systems			**Non-coupling Systems**	
	Occupancy (%frames)			**Occupancy (%frames)**	
A_1R - Gα hydrogen bond	**BnOCPA mode D:Gob**	**BnOCPA mode B:Gob**	**HOCPA:Gob**	**BnOCPA mode D:Goa**	**BnOCPA mode B:Goa**
H317-Q293$^{8.48}$	**1.7**	**0.5**	**2.8**	**6.9**	**10.3**
D263-Q293$^{8.48}$	**0.4**	**0.4**	**1.5**	**9.2**	**0.6**
K294$^{8.49}$-D263	**0.0**	**0.0**	**0.1**	**4.0**	**2.9**
R296$^{8.51}$-D263	**0.1**	**0.5**	**0.0**	**10.7**	**0.0**

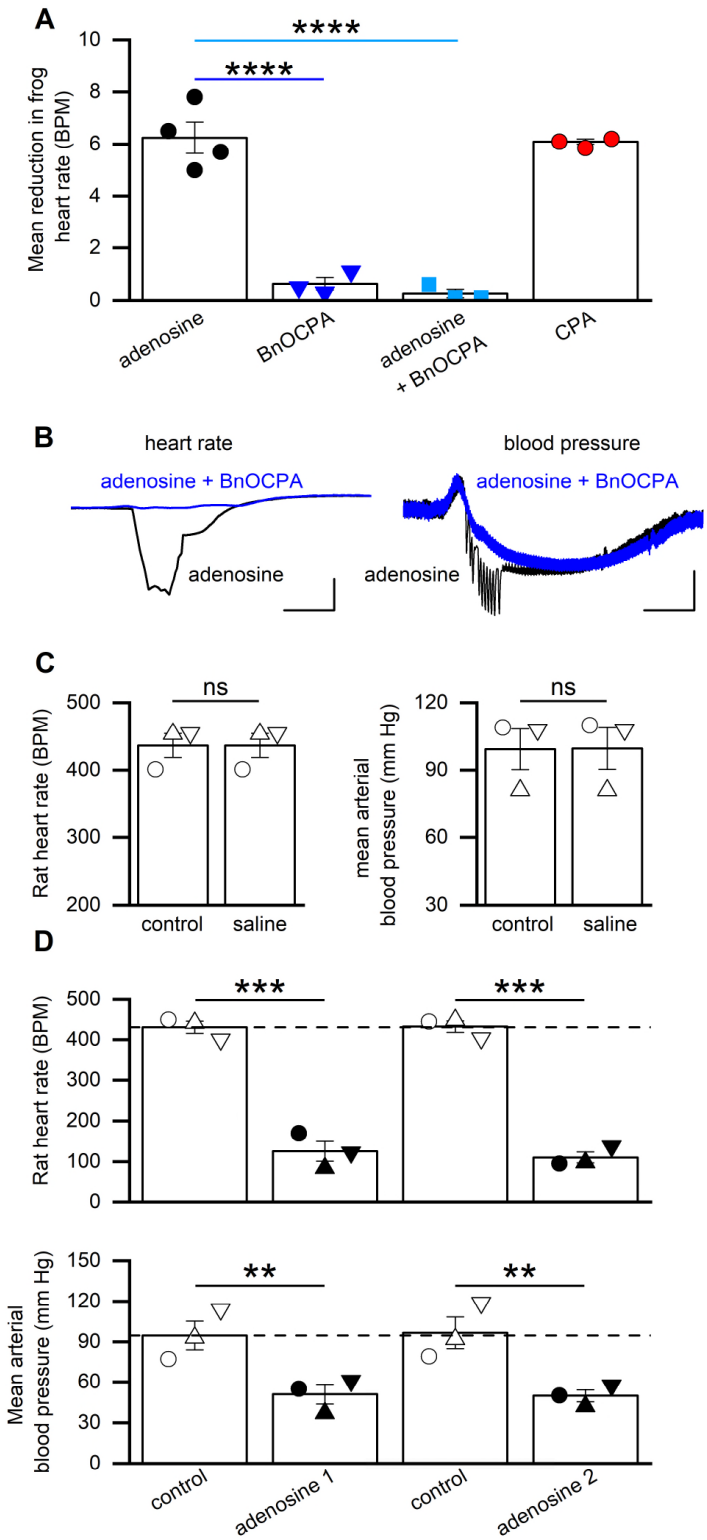

Fig. S9. Actions of BnOCPA on frog heart rate and controls for anesthetised rat experiments.

Fig. S9. Actions of BnOCPA on frog heart rate and controls for anesthetised rat experiments.

(A), Data summary for 3 - 4 isolated frog heart preparations. Application of adenosine (30 μM) reduced heart rate (HR) from 41.8 ± 1.3 BPM to 35.5 ± 1.3 BPM. BnOCPA (300 nM) had no effect on HR (from 42.8 ± 1.2 BPM to 42.1 ± 1.2 BPM; change 0.6 ± 0.2 BPM), an effect that was significantly different from that of adenosine (blue line; $P = 2.22 \times 10^{-5}$). BnOCPA significantly (cyan line; $P = 1.31 \times 10^{-5}$) reduced the effects of subsequent adenosine applications (from a reduction of 6.3 ± 0.6 BPM to 0.3 ± 0.2 BPM). CPA (300 nM) reduced HR by 6.1 ± 0.1 BPM, a value similar to that of adenosine. One way ANOVA on the difference in HR across the 4 conditions ($F(3,9) = 64.64$; $P = 2.070 \times 10^{-6}$), with the reported Bonferroni-corrected P values. **(B)**, Representative traces from a urethane-anaesthetised, spontaneously breathing rat. BnOCPA blocks the effect of adenosine on heart rate (left traces), but only prevents the early phase of adenosine-induced hypotension (right trace). Data taken from the trace in Fig. 5. Scale bars measure 100 BPM or 20 mm Hg and 6 s. **(C)**, Data summary for 3 urethane-anaesthetised, spontaneously breathing rats. Bar charts showing that injection of 0.9 % saline (equivalent volume to drug experiments) had no effect (paired t-test) on either HR ($P = 1$) or mean arterial blood pressure (MAP; $P = 0.422$). **(D)**, Data summary for 3 urethane-anaesthetised, spontaneously breathing rats. Repeated adenosine injections have the same significant effect on HR ($P = 1.40 \times 10^{-4}$ and 1.02×10^{-4}, respectively) and MAP ($P = 0.012$ and 0.008, respectively) and thus show no run down. One-way RM ANOVA for both HR (Greenhouse-Geisser corrected $F(1.97,3.94) = 96.79$, $P = 4.48 \times 10^{-4}$, and MAP ($F(1.10,2.20) = 19.46$, $P = 0.040$) from 3 animals. In **C** and **D**, each symbol represents data from a single rat. ns, not significant; **, $P < 0.02$; ***, $P < 0.001$; ****, $P < 0.0001$.

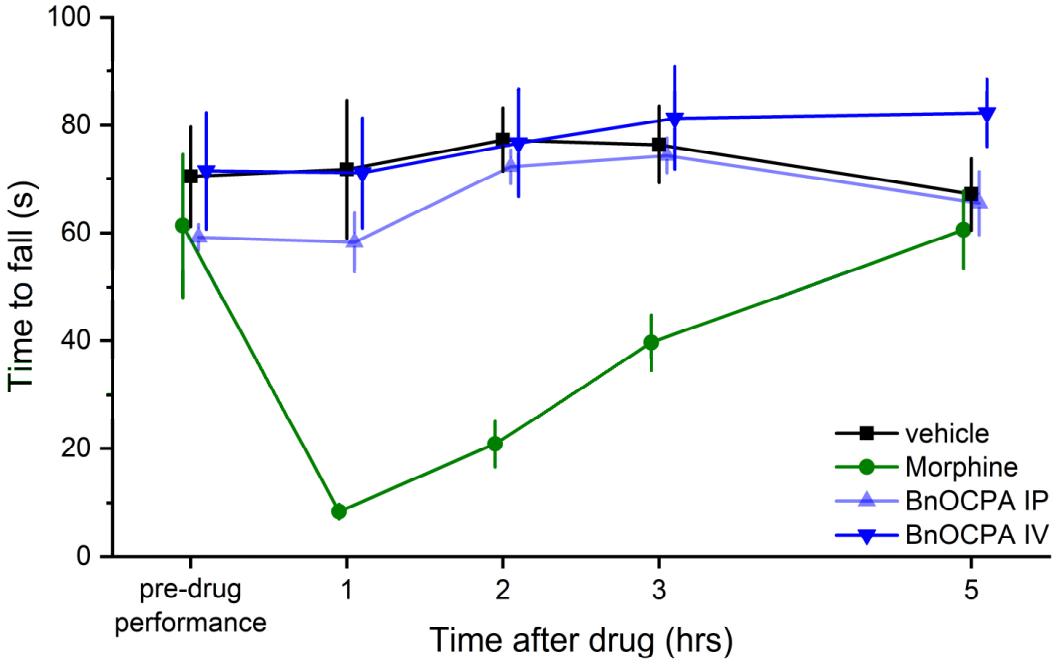

Fig S10 BnOCPA does not impair motor function.

Rats were trained twice in the morning and afternoon for two days (total of 8 practice trials) on an accelerating rotarod (6 to 80 rpm over 170 seconds). BnOCPA was administered IV (n = 6) or IP (n = 6) at 10 µg/kg as per the maximum dose used in the neuropathic pain study (Fig 6E). Morphine (n = 6) was administered at 15 mg/kg subcutaneously. Saline (n = 6) was administered subcutaneously at the same volume as the morphine injection. Rats were tested on the rotarod over a period of 5 hours after injection. BnOCPA did not affect motor function at analgesic doses. Morphine was included as a positive control to validate the assay. Data points are presented as mean ± SEM and are offset for clarity.

Supplemental Figures References

1. Y. Cordeaux, A. P. Ijzerman, S. J. Hill, Coupling of the human A1 adenosine receptor to different heterotrimeric G proteins: evidence for agonist-specific G protein activation. *Br J Pharmacol* **143**, 705-714 (2004).

2. J. G. Baker, S. J. Hill, A comparison of the antagonist affinities for the Gi- and Gs-coupled states of the human adenosine A1-receptor. *J Pharmacol Exp Ther* **320**, 218-228 (2007).

3. S. J. Hill, J. G. Baker, The ups and downs of Gs- to Gi-protein switching. *Br J Pharmacol* **138**, 1188-1189 (2003).